Active Electromagnetic Clutch for Crankshaft Decoupling from a Belt Drive System

applied sciences

MDPI

Article

Active Electromagnetic Clutch for Crankshaft Decoupling from a Belt Drive System

Luis M. Castellanos Molina [1,2,*], Renato Galluzzi [3,*], Shailesh Hegde [1,2], Angelo Bonfitto [1,2], Nicola Amati [1,2], Andrea Tonoli [1,2] and Walter Ventura [4]

1 Center for Automotive Research and Sustainable Mobility (CARS), Politecnico di Torino, 10129 Turin, Italy; shailesh.hegde@polito.it (S.H.); angelo.bonfitto@polito.it (A.B.); nicola.amati@polito.it (N.A.); andrea.tonoli@polito.it (A.T.)
2 Department of Mechanical and Aerospace Engineering, Politecnico di Torino, 10129 Turin, Italy
3 School of Engineering and Sciences, Tecnologico de Monterrey, Mexico City 14380, Mexico
4 Propulsion Solutions srl, 10015 Ivrea, Italy; walter.ventura@dayco.com
* Correspondence: luis.castellanos@polito.it (L.M.C.M.); renato.galluzzi@tec.mx (R.G.)

Abstract: This work presents a novel electromagnetic clutch installed on the crankshaft pulley to decouple the internal combustion engine from the front-end accessory drive of a P0 hybrid electric vehicle. The objective is to supply the air conditioning compressor directly with the belt starter–generator electric machine without dragging the inertia of the engine during engine fuel cut-off phases. This operation yields an improved vehicle energetic efficiency and allows for uninterrupted air conditioning also when the start–stop function is activated. This paper focuses on the mechanical assembly and electromagnetic behavior of the device. Furthermore, two position-sensorless techniques are proposed to estimate the clutch state. The effectiveness of the proposed solution is experimentally validated on a dedicated test bench. Experimental tests demonstrated that the opening and closing phases required 50 and 25 ms, respectively, thereby satisfying the time constraints for switching different operating modes in a vehicle (∼100 ms).

Keywords: hybrid electric vehicle; electromechanical clutch actuator; electromagnet

Citation: Castellanos Molina, L.M.; Galluzzi, R.; Hegde, S.; Bonfitto, A.; Amati, N.; Tonoli, A.; Ventura, W. Active Electromagnetic Clutch for Crankshaft Decoupling from a Belt Drive System. *Appl. Sci.* **2024**, *14*, 4770. https://doi.org/10.3390/app14114770

Academic Editors: Suchao Xie and Junhong Park

Received: 18 March 2024
Revised: 26 May 2024
Accepted: 28 May 2024
Published: 31 May 2024

1. Introduction

In recent years, government regulations on fuel economy and emissions have imposed stringent requirements on the automotive sector. Car manufacturers are being urged to drastically reduce pollution with the goal of achieving more sustainable mobility [1,2]. In this scenario, the incentive to develop alternative powertrain technologies has led to a variety of configurations and architectures for vehicle traction. Alongside the refinement of standard internal combustion engine (ICE) vehicles, alternatives such as pure electric and hybrid electric vehicles have gained popularity. In this context, hybrid electric vehicles have emerged as a transitional solution between electric and traditional ICE vehicles. They combine both ICE and electric machines, leading to various possible powertrain configurations. Ultimately, these solutions contribute to the reduction of fuel consumption and emissions.

The P0 hybrid layout is a configuration in which the standard alternator installed on the front-end accessory drive (FEAD) is replaced by a more powerful and efficient electric machine (EM) that can operate bi-directionally. The EM can recharge the battery through regenerative braking, similar to a traditional alternator. Additionally, it can actively provide boosting torque contributions to assist the ICE during specific transients [3].

The so-called start–stop function automatically shuts off and restarts the ICE in micro-hybrid vehicles to save the energy otherwise spent during idling. In current P0 market solutions, when the start–stop function is active, auxiliary devices attached to the belt transmission, such as the air conditioning (AC) compressor, are turned off. To address

this shortcoming, a clutch device can be installed on the shaft of the ICE to decouple it from the crankshaft pulley and the belt drive system (BDS). In this way, accessories can be operated through the belt transmission using the EM. This action drastically improves the BDS efficiency because the ICE drag losses are removed from the FEAD.

In automotive applications, decoupling subsystems are common practices used to reduce power consumption. Ezemobi et al. [4] proposed the decoupling of the cooling system from the FEAD, demonstrating substantial benefits by electrifying it. The electromagnetic clutch water pumps demonstrated a 4% increase in fuel economy over conventional water pumps when tested through the New European Driving Cycle [5]. Electromagnetic disconnect clutches (EDCs) are used in automotive applications in various hybrid configurations (P0, P1, P2) to decouple the ICE and EM and improve energy management [6]. Similarly, Xu et al. proposed the use of an electromagnetic disconnect friction clutch in P2 architecture to enhance both riding comfort and engine start time in a variety of situations [7]. Huang et al. demonstrated that EDCs may also be utilized in automotive powertrains, where they can be used as a flexible link between the wheel hub and motor for high levels of comfort and smooth power transmission [8,9]. A fractional electromagnetic compound disk brake is another application of electromagnetic actuators, and it demonstrates favorable braking performance [10]. Medei [11] studied the implementation of a passive decoupler to isolate vibrations exchanged between the crankshaft and the FEAD. Fitz and Cali [12] proposed a cam-based mechanism to decouple the alternator pulley from the FEAD. In recent efforts [13,14], Sales et al. carried out an experimental analysis of an alternator equipped with a mechanical decoupling system, which aids in unloading the crankshaft axis in relation to the inertia and electromagnetic field of the alternator. The mechanical decoupling mechanism has been shown to enhance the vehicle's fuel economy by 4.73% during urban driving. Similarly, our earlier research [15] demonstrated that incorporating a FEAD clutch in the BDS results in a 1.3% reduction in fuel consumption when tested using the worldwide harmonized light vehicle test procedure homologation driving cycle. This resulted in a CO_2 emission reduction of 2.3 g/km.

Since the benefits of introducing the aforementioned clutch device have been proven, the present work proposes a novel, highly integrated crankshaft decoupling clutch. This active system is embedded inside the crankshaft pulley to avoid bulky implementations and ensure compatibility with virtually any FEAD architecture. It exploits an electromagnet that provides axial forces for decoupling. The fail-safe operation is guaranteed by return springs that ensure actuation when the functionality of the electromagnetic system is compromised. To identify the clutch state, two position-sensorless strategies are proposed and implemented from voltage and current measurements. These algorithms run in real time on dedicated hardware, which is in constant communication with the vehicle's electronic control unit.

Experimental tests were carried out on the electromagnetic friction clutch of an AC compressor, providing insight into its dynamic characteristics [16]. However, to fulfill the requirement of efficiently powering the AC compressor with an EM instead of an ICE during a vehicle-stop condition, a crankshaft decoupling clutch (CDC) is required. The available literature lacks an in-depth investigation of the CDC to address this objective. Furthermore, most of the research efforts focus on frictional plate-based solutions. In contrast, our study employs a toothed clutch to facilitate integration and compatibility with existing FEAD architecture.

The key contributions of this work are as follows:

1. A novel electromagnetic clutch is presented for a FEAD architecture. In this case, the clutch helps in driving the AC compressor with EM instead of ICE during vehicle stop conditions. To estimate the clutch state, two position-sensorless techniques are also proposed.
2. Experimental tests conducted by means of a dedicated test bench demonstrate the efficacy of the proposed solution, making it a potential solution to be integrated into real vehicles.

The remainder of this work is structured as follows. Section 2 describes the architecture and the mechanical layout of the system. Then, Section 3 outlines the electromagnetic model of the clutch. Section 4 presents two possible position-sensorless strategies to estimate the state of the clutch. Subsequently, Section 5 validates the functionality of the system and the proposed algorithms. Finally, in Section 6, we present our conclusions and discuss future work.

2. System Architecture and Mechanical Assembly

The pulley-clutch system under study operates as an active mechatronic device able to decouple the BDS and the ICE if desired. Installing this device between the belt drive system and the ICE adds a new degree of actuation to the vehicle. When stopping at a traffic light, for instance, the clutch can open. Then, the compressor of the air conditioning can be electrically powered by the EM with no fuel consumption and no ICE inertia involved. This action reduces the amount of time the engine spends idling, thereby reducing fuel consumption and emissions. Figure 1 illustrates the clutch operation and its interaction with the belt drive system and the ICE.

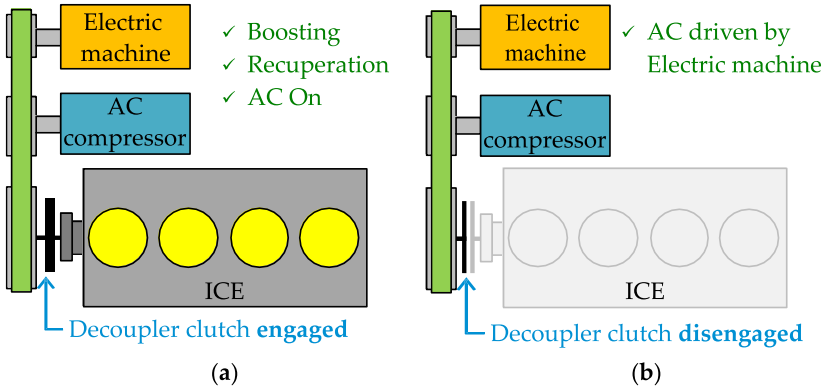

Figure 1. Decoupler clutch operating modes. (**a**) Clutch closed: ICE on and coupled to the belt drive system. In this condition, the electric motor can be used either for boosting (battery discharging) or recuperation (battery charging). (**b**) Clutch open: ICE shut down and its inertia is decoupled from the belt drive system. In this case, the load of the AC compressor is electrically powered.

To achieve this decoupling feature, an active clutch is needed. This actuator is illustrated in Figure 2. It consists of an electromagnetic device placed between the ICE crankshaft and its pulley, which is coupled to the belt drive system. When the clutch is closed, torque and motion transmission are guaranteed through a front gear. When the clutch is open, the pulley (1) can rotate freely with respect to the shaft by means of ball bearings (5). An electromagnet (2) is fixed to the crankcase of the engine to exert forces on a mover (3). This mover slides shaft splines (4). Its front face presents a toothed profile, which couples with a matching pattern (8) on the back of the pulley (1). This configuration benefits from compactness and null slippage when closed. The clutch is normally closed due to the axial force exerted by a conical spring (7), which forces the coupling between the pulley (1) and the mover (3). However, when the electromagnetic coil is energized, a counteracting axial force is produced, thereby compressing the conical spring (7) and opening the coupling between the pulley (1) and the mover (3).

From an electromagnetic standpoint, a controlled current is imposed on the electromagnet to generate a magnetic flux and hence, an attractive magnetic force that opens the clutch. When the hub starts moving, the air gap between the electromagnet and the mover changes from 2.5 mm to the minimum air gap ($\sim$0). A holding current of approximately 2 A is applied to hold the clutch in the open position. To close the clutch, the coil current is set to zero and, hence, the spring force pushes the clutch back to normally closed mode.

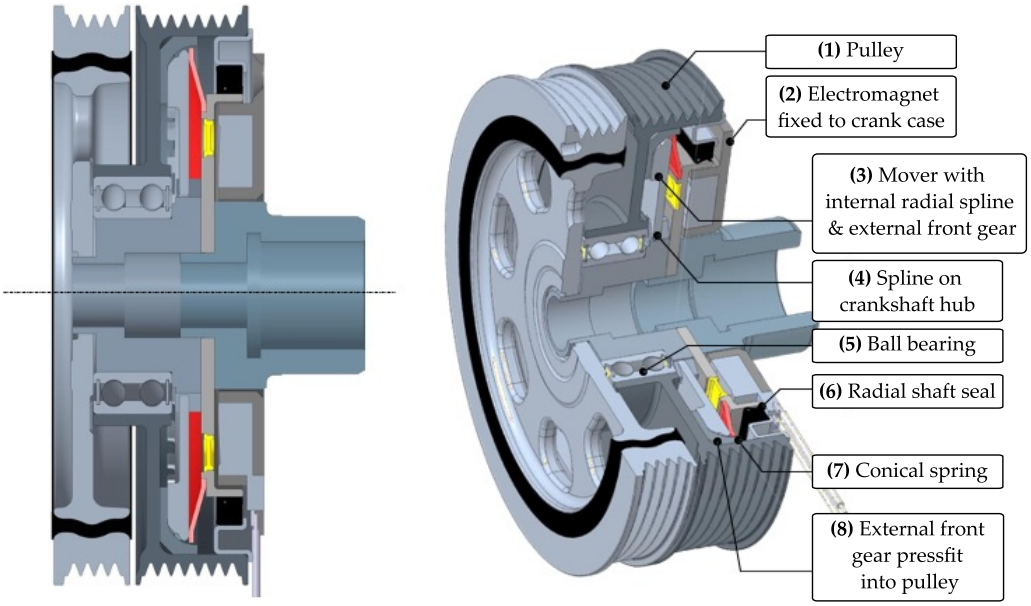

Figure 2. Side and isometric views of the clutch architecture. The pulley shape is exploited to provide an actuator with symmetry with respect to the rotation axis.

3. Electromagnetic Model

The proposed actuator relies on an electromagnet to provide axial force and open the clutch mechanism. Due to the cylindrical shape of the assembly, an electromagnet with axial symmetry is the most suitable. This configuration guarantees a homogeneous axial force pull throughout the active surface of the electromagnet, thus providing robustness against centrifugal and belt forces acting on the pulley. Furthermore, the electromagnetic problem formulation can be simplified into two dimensions, as presented in Figure 3a.

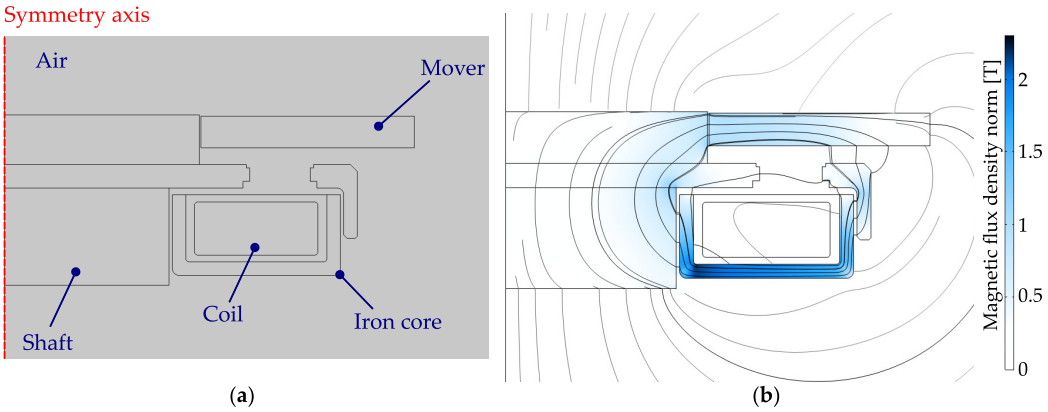

Figure 3. Finite element simulation of the electromagnet with an air gap of 2.5 mm and coil current of 7.2 A. (**a**) Two-dimensional geometry with axial symmetry. (**b**) Magnetic flux density norm distribution (color map), out-of-plane magnetic vector potential (contours).

The parts that constitute the mechanical structure of the actuator are manufactured from soft steel. They also guide the magnetic flux of the electromagnet. A U-shaped iron core is added to close the path of the magnetic circuit and to protect the electromagnetic coil. The thickness of this U-shaped iron core is limited to prevent mechanical interference with the crankcase and to ensure there is sufficient space to house the coil. This coil is a ring-shaped copper winding with 280 turns. The number of turns was chosen to comply with the 12-V battery standard for passenger cars. Relevant parameters of the electromagnetic clutch are summarized in Table 1.

Table 1. Electromagnetic clutch parameters.

Parameter	Value	Unit
Supply voltage (mild hybrid standard)	48	V
Maximum air gap	2.5	mm
Inner diameter	56	mm
Outer diameter	94	mm
Axial thickness	8	mm
Coil current during pull	2	A
Coil current during hold	5	A
Force during pull (max. air gap)	41.3	N
Force during hold (null air gap)	281.6	N
Coil number of turns	280	–
Coil wire gauge	0.56	mm
Coil resistance	4.5	Ω
Coil inductance at max. air gap and null coil current	90.5	mH
Coil inductance at null air gap and coil current of 2 A	40.2	mH

The proposed electromagnetic geometry was simulated in COMSOL Multiphysics at different mover positions, leading to diverse air gap values measured between the mover and the fixed iron plate below it (from zero to 2.5 mm). In each of these positions, the coil was supplied with currents ranging from 0 to 10 A. The finite element model was meshed with 30,000 triangular elements, leading to a skewness-based average element quality of 0.89. Each model simulation takes approximately 30 s to compute.

Figure 3b depicts the magnetic flux density distribution at an air gap of 2.5 mm and a supply current of 7.2 A. It is observed that the proposed U-shaped iron path provides strong saturation in some of its portions, as the saturation point of the iron starts at 1.3 T. Nevertheless, saturation will not lead to an efficiency problem in this device because it operates statically most of the time, i.e., supplied with a constant current. On the contrary, if the iron path is set to a larger thickness, the amount of copper will not be sufficient to provide the necessary attraction force.

Figure 4a,b show the coil flux linkage and electromagnetic force generated, respectively, as a function of the air gap and coil current. These results were obtained with 1066 finite element runs within the input ranges of interest. Since the magnetic flux passes through the air gap twice, the air gap reluctance is involved in the flux path and thus the flux linkage varies not only with the coil current but also with the air gap. Saturation effects are advisable in the flux linkage above 3 A of supply current. The force shows the typical highly nonlinear behavior as a function of input variables.

The data extracted from finite element simulations are useful to enrich a dynamic model of the actuator. By applying Kirchhoff's law to the electromagnet,

$$v_c = \frac{\mathrm{d}}{\mathrm{d}t}\lambda(i_c, g) + i_c R, \tag{1}$$

in which λ is the flux linkage, v_c is the voltage applied to the electromagnet, and R is the coil resistance. Note that the flux linkage changes with both the current of the electromagnet i_c and the air gap g: $\lambda = f_\lambda(i_c, g)$. Accordingly, the force produced by the electromagnet will have the same mapping: $F = f_F(i_c, g)$. This information is compatible with the maps shown in Figure 4.

Using the derivative chain rule yields the following:

$$\frac{\mathrm{d}\lambda}{\mathrm{d}t} = \frac{\partial\lambda}{\partial i_c}\frac{\mathrm{d}i_c}{\mathrm{d}t} + \frac{\partial\lambda}{\partial g}\frac{\mathrm{d}g}{\mathrm{d}t}. \tag{2}$$

Combining (1) and (2) leads to the following:

$$v_c = \underbrace{\left.\frac{\partial \lambda}{\partial i_c}\right|_{(i_c,g)}}_{L(i_c,g)} \frac{\mathrm{d}i_c}{\mathrm{d}t} + \underbrace{\left.\frac{\partial \lambda}{\partial g}\right|_{(i_c,g)} \frac{\mathrm{d}g}{\mathrm{d}t}}_{e_c(i_c,g)} + i_c R; \tag{3}$$

this expression represents the nonlinear electrical behavior of the clutch, in which the resulting inductance L and back-electromotive force (EMF) e_c terms are both functions of i_c and g.

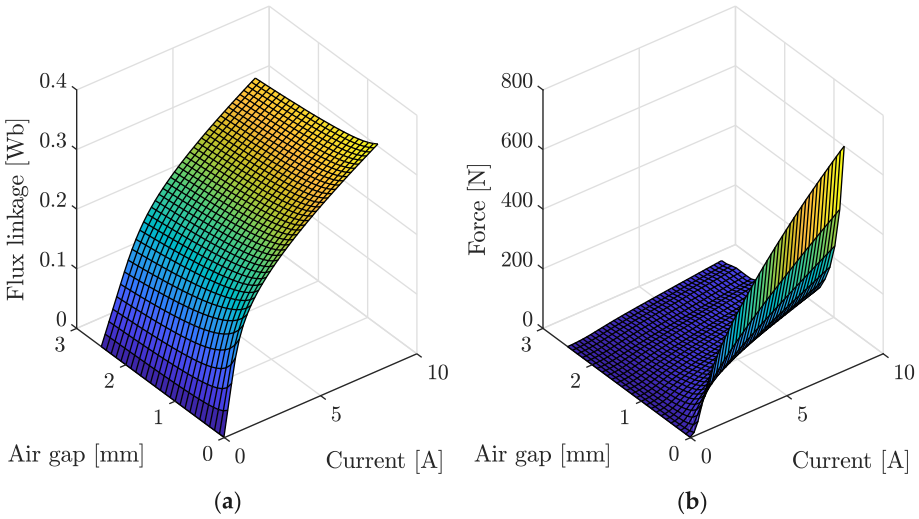

Figure 4. Numerical static FEM simulation variables as a function of the air gap and coil current. (**a**) Coil flux linkage. (**b**) Electromagnetic force.

4. Clutch State Estimation

The fact that both the inductance and the back EMF depend on the clutch position is the core of the two methods proposed for clutch position estimation. Estimating the inductance L when the clutch is at the steady state, i.e., open or closed, can be correlated with the clutch position. On the other hand, when the clutch moves, a non-negligible back-EMF disturbance e_c takes place. This latter contribution is proportional to the air gap speed $\mathrm{d}g/\mathrm{d}t$. When the mover reaches its mechanical limits, either opening or closing, e_c suddenly becomes zero. This produces a noticeable variation in the coil current due to the sudden change in this perturbation.

4.1. Inductance Variation Method

The nominal variation of the inductance as a function of coil current and air gap is plotted in Figure 5. By knowing the inductance at a fixed current, the position of the clutch can be estimated. However, note that the monotonic behavior of the inductance with air gap variation is only guaranteed when the coil current is below 0.6 A.

Figure 5 suggests that the use of the inductance to estimate the air gap is only valid when a small coil current is applied. Thereby, the clutch control unit (CCU) can apply a persistent voltage disturbance that produces a coil current below 0.6 A. When the clutch is closed or open, the disturbance due to back-EMF is not present ($\mathrm{d}g/\mathrm{d}t \approx 0$) and (3) reduces to the following:

$$v_c = L(i_c, g)\frac{\mathrm{d}i_c}{\mathrm{d}t} + i_c R(\Theta). \tag{4}$$

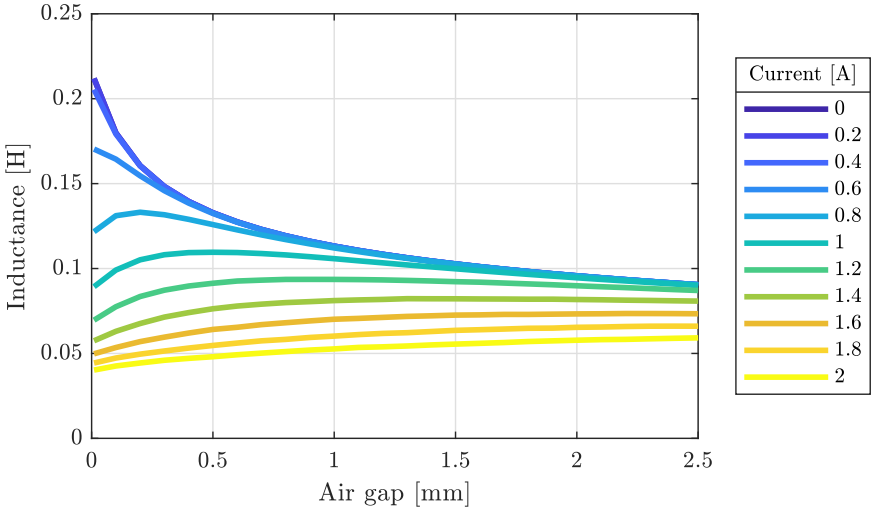

Figure 5. Coil inductance as a function of the air gap, for different coil current values.

The system can be considered a resistive-inductive circuit in which the inductance changes with the coil current and air gap, while the resistance is temperature-dependent (Θ). For a short time frame, both the inductance and the resistance are assumed to be constant. Rewriting (4) in the Laplace form yields the following:

$$\frac{i_c(s)}{v_c(s)} = \frac{1}{sL + R}. \tag{5}$$

For a practical implementation in the CCU, a linear difference equation is obtained using Tustin's discretization method:

$$a_1 i_c z^{-1} + a_0 i_c = b_1 v_c z^{-1} + b_0 v_c, \tag{6}$$

where $b_0 = b_1 = T_s$ is the sampling time and

$$a_0 = 2L + RT_s \tag{7a}$$
$$a_1 = RT_s - 2L. \tag{7b}$$

At time instant k, and using N past measurements of the coil current i_c and voltage v_c, expression (6) is arranged as follows:

$$\underbrace{\begin{bmatrix} i_{c,k} & i_{c,k-1} \\ i_{c,k-1} & i_{c,k-2} \\ \vdots & \vdots \\ i_{c,k-N+1} & i_{c,k-N} \end{bmatrix}}_{A} \begin{bmatrix} a_0 \\ a_1 \end{bmatrix} = \underbrace{\begin{bmatrix} b_1 v_{c,k-1} + b_0 v_{c,k} \\ \vdots \\ b_1 v_{c,k-N} + b_0 v_{c,k-N+1} \end{bmatrix}}_{b} + \boldsymbol{\omega}. \tag{8}$$

The vector $\boldsymbol{\omega} = [\omega_1, \cdots, \omega_N]^\intercal$ has been added to lump the uncertainty due to the measurement error. Since A and b are known, the minimum mean square error is used to obtain the coefficients a_0 and a_1. Then, the equation system in (7) is solved to obtain L and R.

Finally, the estimated inductance is used to evaluate the clutch state. For instance, when the clutch is correctly closed ($g = 2.5$ mm) and the excitation current is below 0.6 A, it is seen from Figure 5 that the inductance is confined to approximately 90 mH. Different inductance values would indicate a clutch malfunction.

4.2. Back-EMF Disturbance Method

To open the clutch, a coil current between 5 to 6 A is needed to overcome friction and inertial contributions to open the toothed profile and pull the mover. This current is applied for 0.2 s. Then, a holding current of 2 A is used to maintain the clutch open. Due to iron saturation, the previously presented inductance estimation method is not a suitable candidate to estimate the state of the clutch. Note from Figure 5 that the variation of the inductance with the clutch air gap is not indicative when the coil current is larger than 0.6 A. However, the back-EMF voltage is not negligible when the clutch is opening. This disturbance is here exploited to estimate the clutch state.

In fact, there is an increase in the back-EMF voltage (e_c) when the clutch is opening/closing. By converse, e_c becomes zero when the clutch hub is hardly stopped due to mechanical contact at both stroke ends (minimum/maximum air gap). This sudden change in back-EMF generates a strong variation of the coil current at the instant of the impact. Thus, monitoring both e_c and i_c in real time could be useful to identify the effectiveness of the clutch operation. The proper estimate of the back-EMF is challenging to obtain because it presents highly nonlinear behavior at the instant of the impact and it is not a persistent disturbance.

5. Experimental Validation

The experimental tests were conducted using the belt test bench shown in Figure 6. The BDS is constituted by three pulleys: (1) belt starter–generator, (2) AC compressor, and (3) crankshaft. The clutch pulley device is installed on an e-motor that reproduces the crankshaft speed profile. When the clutch is open, the belt starter–generator electric machine drives the AC compressor. To identify the closing and opening phases, a microphone (4) measures the acoustic noise produced by these events.

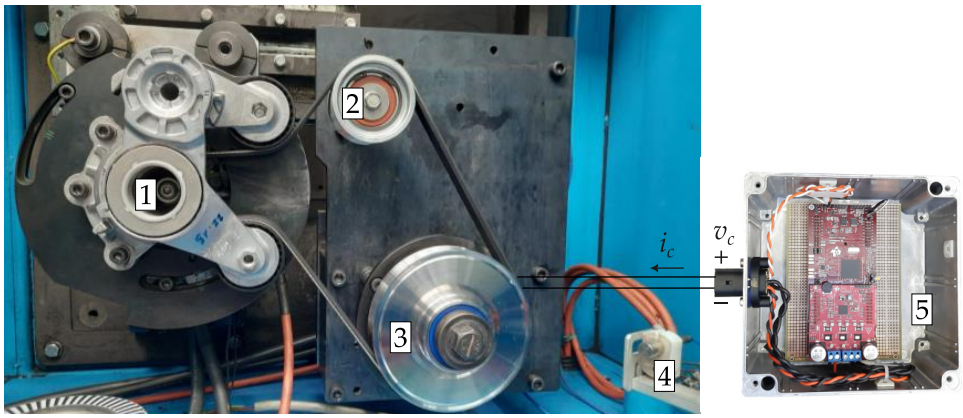

Figure 6. Testbed for experimental characterization of the clutch. (1) Belt starter–generator electric machine with belt tensioner on top, (2) AC compressor pulley, (3) crankshaft pulley with electromagnetic clutch installed, (4) microphone to measure the noise of the impact when the clutch changes its state, (5) clutch control unit (CCU).

The clutch control unit (CCU) is based on a Texas Instruments F28379 processing unit together with a BOOSTXL-DRV8323RS power module. The latter is a fully configurable 3-phase inverter with shunt current sensors incorporated. The power module is used as an H-bridge to supply the electromagnet with a modulated voltage and guarantee the required current profiles on the electromagnet. A proportional–integral (PI) controller is implemented to yield current tracking on the electromagnet. The CCU communicates via a controller area network (CAN) with the vehicle control unit. It receives the clutch commands and feeds back the clutch state. The software is deployed directly from the MATLAB environment using the embedded Coder support package for Texas Instruments C2000 Processors. The layout of the CCU is depicted in Figure 7.

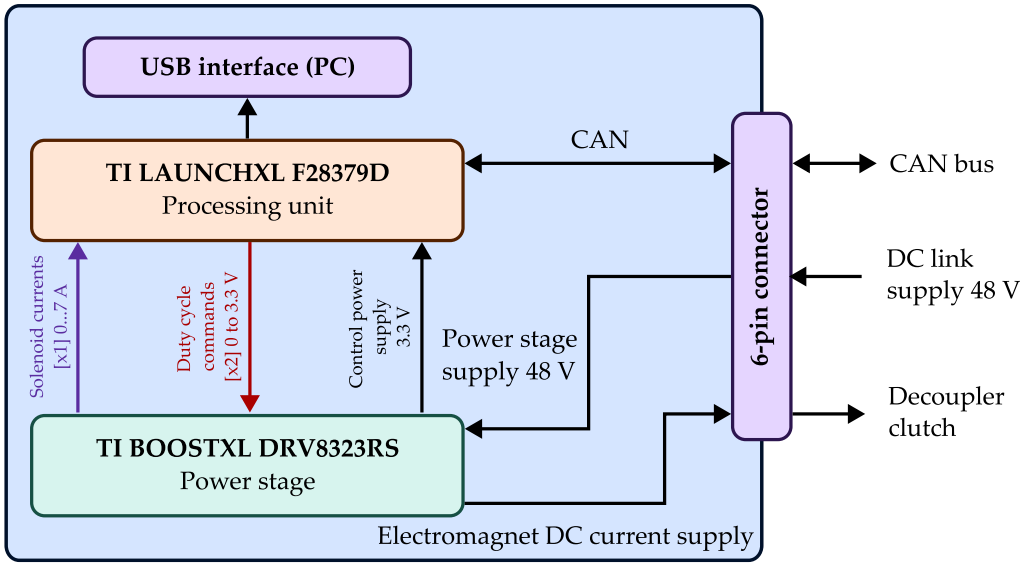

Figure 7. Layout of the clutch control unit (CCU).

5.1. Clutch Functionality Tests

Figure 8 depicts a typical actuation task for the electromagnetic clutch. The system is normally closed. A disable (DIS) signal is received at $t \approx 0.3$ s. The coil current PI control is set to track a pull current reference of 5 A. When this setpoint is reached, the clutch command is set to zero. The current generates a magnetic force that pulls the mover and opens the clutch. Strong disturbances in the current are appreciated at the instant of the impact. This is due to the fast variation of the hub speed when it reaches the mechanical stroke limits. After a time interval of 0.2 s, the coil current setpoint is lowered to a hold value of 2 A to keep the clutch in open mode. The value of the current is lower in this case because the electromagnetic force counteracts only the elastic reaction of the conical spring.

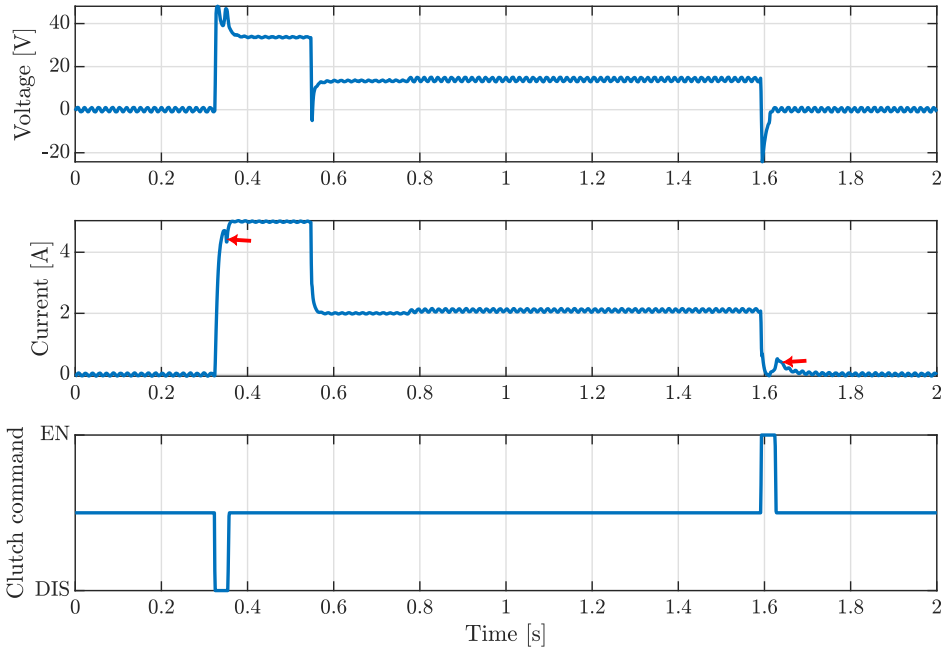

Figure 8. Clutch operation time history: Electromagnetic voltage (**top**), current (**middle**), and clutch command (**bottom**). Current perturbations due to back-EMF are highlighted during closing and opening with arrows.

At 1.6 s, an enable (EN) command is received. The current reference is set to zero. Thus, the return spring releases its energy to set back the mover. When the mover reaches its end stroke, a back-EMF disturbance yields a variation in the coil current, which then approaches zero.

A realistic working condition is reproduced by means of the described test bench in Figure 9. During the initial phase, the clutch is closed and transmits power to the belt starter–generator through the belt transmission. This is shown by the angular speed of the machine and the null current in the clutch coil. At 10 s, when the vehicle has already stopped, the clutch is opened: A pull current is briefly applied and then lowered to a holding value. Subsequently, the electric machine powers the AC compressor while the ICE is decoupled and off. Finally, the electric machine stops and the clutch is closed to restore BDS functionality.

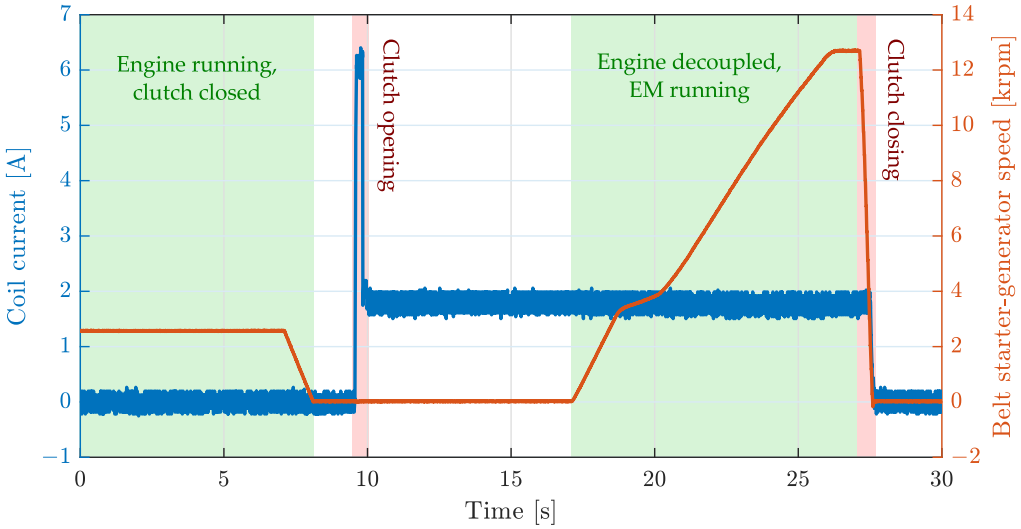

Figure 9. Test bench emulation of a typical working condition of the clutch within a belt drive system. The belt starter–generator electric machine (EM) was driven up to its maximum speed (∼12,000 rpm) to stress the functionality of the clutch.

Note that when the engine is decoupled, the belt starter–generator electric machine (EM) is driven up to maximum speed. To re-establish a traditional BDS, the EM is stopped at max. deceleration and the clutch is closed again. In this worst-case condition, each of these two phases has a maximum actuation time requirement of 100 ms fulfilled in both cases.

5.2. Inductance Variation Method Tests

Before implementing the inductance estimation method on the CCU, a preliminary experimental Fourier analysis was conducted to investigate the variation of the inductance over a frequency range between 1 and 100 Hz. Tests were performed by applying a biased voltage sweep with the clutch manually forced to stay open (minimum air gap) or closed (maximum air gap). This test was repeated at three current bias values: 1, 1.4, and 2.8 A. As seen in Figure 10, determining the clutch state via inductance variation becomes difficult due to magnetic saturation, even at the lowest bias current. These results support the preliminary numerical analysis shown in Figure 5.

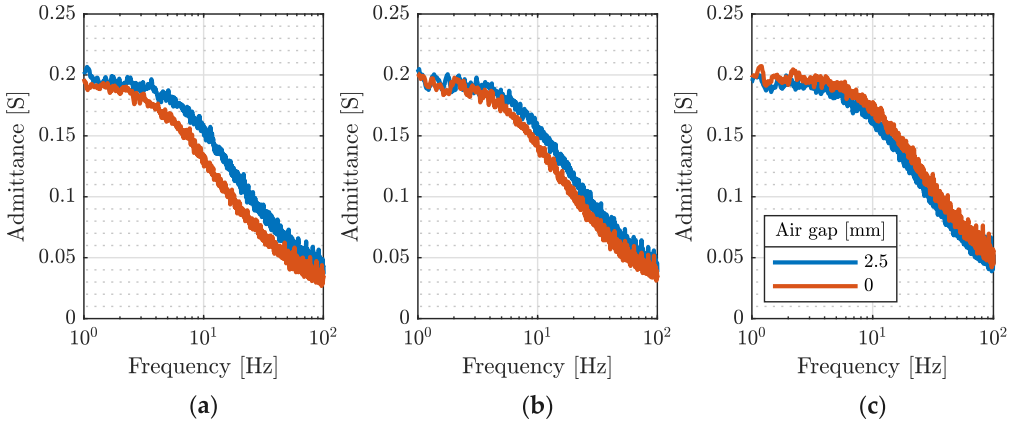

Figure 10. Frequency response at different air gaps. Tests were conducted with average coil currents of (**a**) 1.0 A, (**b**) 1.4 A, and (**c**) 2.8 A. The inductance variation becomes smaller when the drive current increases. The evaluation of the clutch state from the inductance variation is difficult to achieve when the coil current is larger than 1.4 A due to magnetic saturation.

5.3. Back-EMF Disturbance Method Tests

Figure 11 shows the electromagnetic current profile disturbed with the back-EMF voltage during the (a) opening and (b) closing phases. In both cases, the current fluctuation is 0.3 A, which is easily measured through the available shunt resistance sensors in the CCU. A microphone is used to measure the impact noise, this helps determine the actuation timing. This acoustic measurement is only available for evaluation purposes; it is not used during normal vehicle operation. Interestingly, the opening phase lasts less than 50 ms, whereas the closing phase lasts 25 ms which is notably lower than the reaction time needed to change the operation mode of the vehicle (∼100 ms).

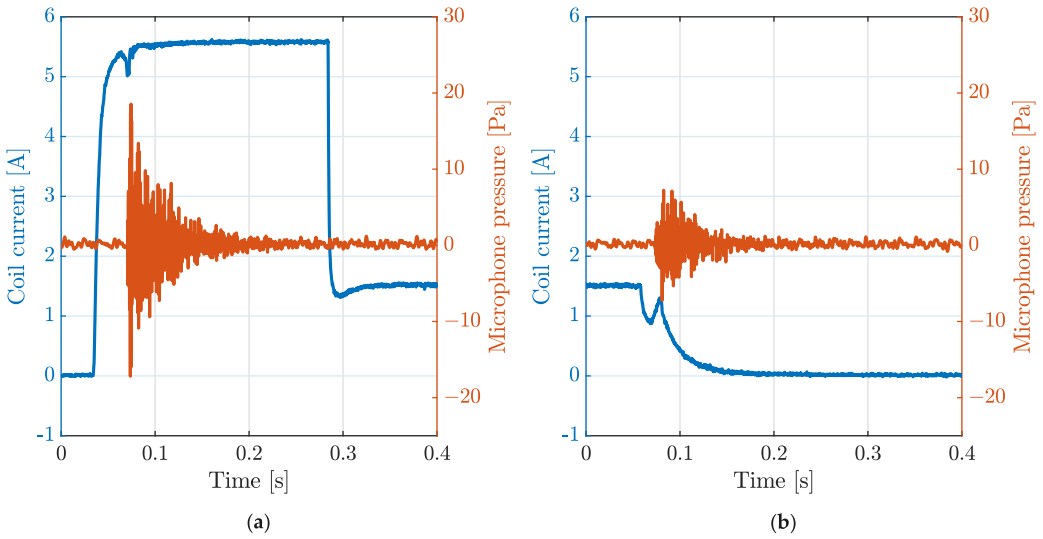

Figure 11. Coil current and microphone pressure when the clutch is (**a**) opening (clutch moving towards minimum air gap), and (**b**) closing (clutch moving towards maximum air gap). The coil current is clearly disturbed at the instant when the hub drastically stops moving due to mechanical contact. A microphone is used to determine the instant of the impact.

6. Conclusions

This work presents a novel electromagnetic clutch that decouples the crankshaft from the belt driven system. It provides the possibility for AC extension during the start–stop operation, avoiding the engine drag torque. The working principle of the clutch and its electromagnetic behavior are modeled. Experimental tests demonstrate the functionality of the proposed actuator. Two procedures to estimate the clutch state are described. The

first, focused on the inductance estimate, can potentially give a more precise estimate of the air gap but is severely hindered by saturation. The second one employs the current disturbance due to back-EMF to identify the clutch state. Although not particularly precise, this latter technique can identify the clutch state as binary information.

The experimental test validated that the opening and closing phases required 50 and 25 ms, respectively. As a result, the time constraints of 100 ms for switching between operating modes in a vehicle were satisfied. Real-time deployment of these algorithms is carried out on a clutch control unit. The experimental test was undertaken with an active electromagnetic clutch paired with the control control unit, making it an effective choice for automotive applications. From a functional safety perspective, both strategies can be combined to provide a redundant state estimation scheme.

Further developments of this project include the installation of the actuator in a vehicle and its use to implement and assess energy-saving strategies.

Author Contributions: Conceptualization, L.M.C.M., R.G., A.B., N.A., A.T. and W.V.; methodology, L.M.C.M., R.G., S.H., A.B. and W.V.; software, L.M.C.M.; validation, L.M.C.M.; formal analysis, L.M.C.M. and R.G.; investigation, L.M.C.M., R.G. and S.H.; resources, N.A., A.T. and W.V.; data curation, L.M.C.M. and R.G.; writing—original draft preparation, L.M.C.M. and R.G.; writing—review and editing, S.H., A.B., N.A., A.T. and W.V.; visualization, L.M.C.M. and R.G.; supervision, N.A., A.T. and W.V.; project administration, N.A., A.T. and W.V.; funding acquisition, N.A., A.T. and W.V. All authors have read and agreed to the published version of the manuscript.

Funding: This study was carried out within the Ministerial Decree no. 1062/2021 and received funding from the FSE REACT-EU-PON Ricerca e Innovazione 2014–2020. This manuscript reflects only the authors' views and opinions, neither the European Union nor the European Commission can be considered responsible for them.

Institutional Review Board Statement: Not applicable.

Informed Consent Statement: Not applicable.

Data Availability Statement: The datasets presented in this article are not readily available because they are protected by a collaboration agreement between the interested parties.

Conflicts of Interest: The authors declare no conflicts of interest.

Abbreviations

The following abbreviations are used in this manuscript:

AC	air conditioning
BDS	belt drive system
CAN	controller area network
CCU	clutch control unit
DIS	disable coupling with engine
EM	electric machine
EMF	electromotive force
EN	enable coupling with engine
FEAD	front-end accessory drive
ICE	internal combustion engine
PI	proportional–integral

References

1. European Commission. Communication from the Commission to the European Parliament, the Council, the European Economic and Social Committee and the Committee of the Regions 'Fit for 55': Delivering the EU's 2030 Climate Target on the Way to Climate Neutrality. 2021. Available online: https://eur-lex.europa.eu/legal-content/EN/TXT/?uri=CELEX%3A52021DC0550 (accessed on 1 March 2024).

2. Regulation—2019/631—EN—EUR-Lex. Regulation (EU) 2019/631 of the European Parliament and of the Council of 17 April 2019 Setting CO_2 Emission Performance Standards for New Passenger Cars and for New Light Commercial Vehicles, and Repealing Regulations (EC) No 443/2009 and (EU) No 510/2011 (Recast) (Text with EEA Relevance). Available online: https://eur-lex.europa.eu/legal-content/EN/TXT/?uri=CELEX%3A32019R0631 (accessed on 1 March 2024).
3. di Napoli, M.; Galluzzi, R.; Zenerino, E.C.; Tonoli, A.; Amati, N. Investigation on the performances of a twin arm tensioning device. *Proc. Inst. Mech. Eng. Part D J. Automob. Eng.* **2019**, *233*, 1687–1697. [CrossRef]
4. Ezemobi, E.N.; Ruzimov, S.; Bonfitto, A.; Tonoli, A.; Amati, N. Energy Savings from Electrification of Cooling System. In Proceedings of the ASME 2020 International Design Engineering Technical Conferences and Computers and Information in Engineering Conference, Virtual, 17–19 August 2020; Volume 4, p. V004T04A024. [CrossRef]
5. Shin, Y.H.; Kim, S.C.; Kim, M.S. Use of electromagnetic clutch water pumps in vehicle engine cooling systems to reduce fuel consumption. *Energy* **2013**, 57, *624–631. [CrossRef]*
6. *Böhme, T.J.; Frank, B.* Hybrid Systems, Optimal Control and Hybrid Vehicles: Theory, Methods and Applications; Advances in Industrial Control; Springer International Publishing: Cham, Switzerland, 2017. [CrossRef]
7. Xu, X.; Liang, Y.; Jordan, M.; Tenberge, P.; Dong, P. Optimized control of engine start assisted by the disconnect clutch in a P2 hybrid automatic transmission. *Mech. Syst. Signal Process.* **2019**, *124*, 313–329. [CrossRef]
8. Yu, W.; Gu, C. Design and implementation of an electromagnetic clutch system for hub motors. In Proceedings of the 2014 17th International Conference on Electrical Machines and Systems (ICEMS), Hangzhou, China, 22–25 October 2014; IEEE: Piscataway, NJ, USA, 2014; pp. 1183–1186.
9. Yu, W.; Gu, C. Dynamic analysis of a novel clutch system for in-wheel motor drive electric vehicles. *IET Electr. Power Appl.* **2017**, *11*, 90–98. [CrossRef]
10. Huang, S.; Bao, J.; Ge, S.; Yin, Y.; Liu, T. Design of a frictional–electromagnetic compound disk brake for automotives. *Proc. Inst. Mech. Eng. Part D J. Autom. Eng.* **2020**, *234*, 1113–1122. [CrossRef]
11. Medei, S. Modelling and Design of a Crankshaft Decoupler for Internal Combustion Engines. Master's Thesis, University of Illinois at Chicago, Chicago, IL, USA, 2012.
12. Fitz, F.A.; Cali, C.P. Controlled Alternator Decoupling for Reduced Noise and Vibration. In Proceedings of the SAE 2010 World Congress & Exhibition, Detroit, MI, USA, 13–15 April 2010; pp. 1–8. [CrossRef]
13. Sales, L.C.M.; Sousa, J.M.S.; Monteiro, L.G.C.; Rodrigues, J.P.; Borges, F.R. Experimental comparative analysis of the combined Stop & Start and alternator with mechanical decoupling strategies. In Proceedings of the 2018 SAE Brasil Congress & Exhibition, Grapevine, TE, USA, 15–18 September 2018; p. 2018-36-0341. [CrossRef]
14. Sales, L.C.M.; Pacheco, E.P.; Monteiro, L.G.C.; Souza, L.G.; Mota, M.S. Evaluation of the Influence of an Alternator with Mechanical Decoupling on Energy Consumption and CO_2 Emission in a Flex Fuel Vehicle. In Proceedings of the 26th SAE BRASIL Inernational Congress and Display, São Paulo, Brasil, 7–9 November 2017; p. 2017-36-0116. [CrossRef]
15. Hegde, S.; Castellanos Molina, L.M.; Bonfitto, A.; Galluzzi, R.; Amati, N.; Tonoli, A. Crankshaft Decoupling Effects on Fuel Economy in HEV-P0. In Proceedings of the Volume 1: 24th International Conference on Advanced Vehicle Technologies (AVT), St. Louis, MO, USA, 14–17 August 2022; p. V001T01A016. [CrossRef]
16. Diao, Z.; Zhang, Y.; Li, C.; Liu, X.; Liu, Z. Dynamic Characteristics of an Automotive Air-Conditioning Electromagnetic Clutch. *Processes* **2024**, *12*, 80. [CrossRef]